Studying the real-time interplay between triglyceride digestion and lipophilic micronutrient bioaccessibility using droplet microfluidics. 1 lab on a chip method

Thanh Hoang, Mélanie Nguyen, Marc Marquis, Sébastien Anton, Hoang Thanh Nguyen, Mélanie Marquis, Marc Anton, S. Marze

Studying the real-time interplay between triglyceride digestion and lipophilic micronutrient bioaccessibility using droplet microfluidics. 1 Lab on a chip method

Hoang Thanh NGUYEN, Mélanie MARQUIS, Marc ANTON, Sébastien MARZE

Biopolymères Interactions Assemblages, INRA, 44300 Nantes, France

Abstract

This article is the first part of a series reporting on real-time digestion kinetics of triglyceride droplets containing different lipophilic micronutrients. This part focuses on the design, fabrication, and operation of a polydimethylsiloxane microfluidic device which enables the generation and digestion of oil droplets. The micro-channels were made hydrophilic to obtain oil droplets in an aqueous continuous phase. Optimized chip design and outlet control were implemented to provide efficient oil droplet generation, manipulation, and immobilization on a single chip. Highly monodisperse oil droplets were generated, immobilized in an array of traps and monitored in real time by fluorescence using a confocal microscopy method. The device was used to study the kinetics of beta-carotene release during tricaprylin digestion (intestinal lipolysis and micellar solubilization). The effect of the gastric phase on beta-carotene degradation was also investigated using the same method.

1. Introduction

Over the past decades, the development of technologies based on microfluidics has expanded in analysis and research domains (Huebner et al., 2009; Šalić, Tušek, & Zelić, 2012). Indeed, the use of micro-scale experimental devices involves small sample volumes with a high surface-volume ratio that allows reduction of costs and rapid kinetics study. In addition, the optical transmission of the materials commonly used in microfluidics (mostly polydimethylsiloxane (PDMS), poly(methyl methacrylate) (PMMA), and glass) provides high flexibility to use external light-based analysis techniques for real-time monitoring (Desai & Zaman, 2015; Heus et al., 2010; Mongersun, Smeenk, Pratx, Asuri, & Abbyad, 2016; Windbergs & Weitz, 2011). With the trend of further reducing the sample volume, droplet microfluidics was developed. In this technique, each droplet is used as an independent micro-reactor of pico- to nano- litre scale (Huebner et al., 2009; Huebner, Abell, Huck, Baroud, & Hollfelder, 2011; Mongersun et al., 2016). However, most of the studies are based

on water droplets, while oil droplets are rarely explored. In particular, lipid droplets containing lipophilic micronutrients or hydrophobic drugs were rarely investigated.

On the contrary, *in vitro* digestion of lipid and lipophilic bioactive molecules is extensively carried out using emulsions (Marze, 2015; Li, Kim, Park, & McClements, 2012). Nevertheless, even in a “simple” system such as emulsion, studying mechanisms is still challenging due to many interactions involved simultaneously. Emulsion digestion is indeed influenced by many physicochemical characteristics which are difficult to control. Moreover, real-time kinetics studies of lipid/lipophilic molecules digestion were rarely achieved using the conventional emulsion approach.

Those issues can be solved using droplet microfluidics. In that context, the use of the lipid droplet microfluidic digestion system recently developed by Marze et al. showed equivalent results to those obtained from static *in vitro* digestion of emulsions (Marze, Algaba, & Marquis, 2014). Then, Scheuble et al. reported a similar approach based on lipid droplet digestion with multiple oil droplets trapping to study the coalescence effect (Scheuble et al., 2017). Using various lipid droplets in a microfluidic device can be seen as a potential screening approach not only for the digestion of lipids but also for the release of lipophilic bioactive molecules. However, several difficulties needed to be solved to make droplet microfluidics an experimental standard for lipid studies in micro-reactors. First, the micro-channel surface has to be hydrophilic to enable oil droplet generation and manipulation. As most microfluidic materials are natively hydrophobic, a chemical treatment is required to obtain a persistent hydrophilic surface (He et al., 2011; Marze et al., 2014; Tan, Xu, Li, & Luo, 2008; Wang, Lu, Xu, & Luo, 2009). The second difficultly is the control of the oil droplet generation, which may undergo flow instabilities due to the high viscosity of edible oils compared to that of water (Marze et al., 2014). Finally, a proper optical setup is needed to quantify the kinetics of lipophilic molecules in real time.

In this article, we present an optimized microfluidic platform to overcome these limitations. A single PDMS chip based on a microfluidic device with hydrophilic surface modification was developed to generate and manipulate monodisperse oil droplets that are immobilized in an array of traps. The hydrophilic treatment and device storage were optimized to obtain a long hydrophilicity persistency of the channel surface. The oil droplet generation and flow were stabilized by an open-close procedure of the outlets, with no extra devices or valves required. The use of this platform is illustrated by examples of single and multiple droplet trapping. Then, the implementation of a confocal fluorescence microscope setup for real-time monitoring is illustrated by the kinetics of beta-carotene release from tricaprylin droplets

during digestion. The kinetics of beta-carotene degradation in gastric conditions is also presented, monitored in real time using this setup as well.

2. Experimental Section

2.1. Materials

The negative photoresist (SU8-2100) was from MicroChem Corp, PDMS (RTV615) was from Eleco Produits, polytetrafluoroethylene (PTFE) tubes (11919445) were from Fisher Scientific, stainless steel tubes (Coop 23G/15 mm) and Luer lock needles (LS22) were from Phymep. The other chemicals were provided by Sigma-Aldrich: propylene glycol methyl ether acetate (PGMEA), benzophenone, acrylic acid, pancreatic lipase (L3126, lipase from porcine pancreas type II, 1.6-8.3 U mg^{-1}), sodium glycodeoxycholate (G9910), tricaprylin (T9126), beta-carotene (22040), Amano lipase A (534781, fungal lipase from *Aspergillus niger*, 12 U mg^{-1}, protease activity $\leq$ 2.5 U mg^{-1}), pepsin (P7012, from porcine gastric mucosa, 2500 U mg^{-1}). β-lactoglobulin was purified from whey protein isolate in our laboratory. Milli-Q water with an electrical resistivity of 18.2 MΩ was used for all solution preparations.

2.2. Microfluidic Device

The preparation of the PDMS microfluidic device is based on soft lithography techniques using silicon wafer for the master (Whitesides, Ostuni, Takayama, Jiang, & Ingber, 2001).

2.2.1. Photomask design. We used the Adobe Illustrator software to draw the mask design which was then printed out as a photo mask by high resolution printing.

2.2.2. Master fabrication. The master was made using photolithography techniques. A thin layer of negative photoresist was coated on a silicon wafer using a spin-coater (SPIN150, SPSEurope). This was prebaked for 5 min at 65 ^{0}C followed with 20 min at 95 ^{0}C before being exposed to UV light (365 nm) for 40 s through the photomask by a UV LED masker (UV-KUB 2, Kloé). The post-baking was done for 5 min at 65 ^{0}C followed by 10 min at 95 ^{0}C. Finally, the master with microstructures of 120 µm in height was obtained by development with a solution of PGMEA for 20-30 min. Propanol was used to wash excess products of development, resulting in a clean master.

2.2.3. PDMS chip. The device was fabricated using similar techniques found in Marquis et al. (Marquis, Renard, & Cathala, 2012). One device is composed of two PDMS parts bonded by the gradient technique. First, two PDMS/crosslinker mixtures (10% or 5% crosslinker) were poured on the master and in a Petri dish, respectively. Then, both parts were degassed in a vacuum chamber (50 mbar). After the degassing step, both parts were cured at 70 ^{0}C for 30 min. The cured PDMS (10% crosslinker) was cut and peeled off the master before access

holes for inlets and outlets were punched through PDMS. Then, this PDMS part was cleaned and assembled with the 5% crosslinker PDMS in the Petri dish by curing at 70 ^{0}C for 1 hour. Stainless steel tubes were inserted in the access holes, reinforced by plastic rings filled with cured PDMS (5% of crosslinker). Finally, the device was cured overnight at 70 ^{0}C and the stainless steel tubes were replaced by new ones for the inlets/outlets of the device. The design of the chip is shown in fig. 1a.

2.2.4. Hydrophilic treatment. PDMS surface is natively hydrophobic (water contact angle > 100°) (Mata, Fleischman, & Roy, 2005). In this work, the PDMS device was used to generate and trap oil droplets in an aqueous continuous phase. Thus, the surface of PDMS channel needed to be modified. A hydrophilic treatment was achieved by UV-initiated graft polymerization of acrylic acid as proposed by Schneider et al. (Schneider, Willaime, Tran, Rezgui, & Tabeling, 2010). The first step was the injection of a 10% benzophenone in acetone at a flow rate of 200 µL min^{-1} for 10 min. Then, the remaining solution was blown out by air flow and the device was placed under vacuum (85 mbar) for 35 min before the injection of a 20% acrylic acid aqueous solution at a flow rate of 200 µL min^{-1} for 5 min. Next, the acrylic acid solution was sealed into the device by closing access holes. The device was illuminated with UV for 5 min using the UV LED masker. Finally, the device was cleaned by successive flow of ethanol and water (pH 11) at 200 µL min^{-1} for 1 hour. After the hydrophilic treatment, the device was put inside a plastic bottle filled with distilled water (pH 11) and stored at 4 ^{o}C to maintain the hydrophilicity of the channel surface.

2.3. Droplet Generation and trapping

All fluid flows were generated and controlled by syringe pumps 11 elite (Harvard Apparatus) with glass syringes connected to the inlets of device by a Luer lock needle and PTFE tubes. During the device operation, the outlets and inlets of the device were temporarily blocked by a piece of PTFE tube filled with cured PDMS.

For droplet generation, the microfluidic device was placed under an IX51 inverted microscope (Olympus) with a 4× objective. First, the continuous phase (7.5 mg mL^{-1} β-lactoglobulin in 10 mM NaH_2PO_4 adjusted to pH 7.0) and the oil phase (tricaprylin) were injected into the micro-channels via inlet 1 at a flow rate of 150 µL min^{-1}, and via inlet 2 at a flow rate of 4 µL min^{-1}, respectively. Then, the flow rate was decreased to 50 µL min^{-1} for the continuous phase and to 1 µL min^{-1} for the oil phase to generate oil droplets of 100 µm. Initially, outlet 4 was blocked, leading the first oil droplets to the waste tank via outlet 3. When the desired oil droplet size was reached (100 µm), outlet 4 was opened and outlet 3 was blocked, leading the oil droplets to the chamber. When most of the chamber traps were filled with one oil droplet, the oil flow was stopped and the aqueous continuous phase flow was increased to 100 µL min^{-1} to wash out any untrapped droplets of the chamber. Next,

outlet 3 was opened and outlet 4 was blocked to prevent any undesirable large oil droplets from entering the chamber.

2.4. Droplet digestion

Initially, monodisperse tricaprylin droplets (100 µm in diameter) with added 0.2 wt% beta-carotene were generated and trapped in the microfluidic device as described above. Then, all four access tubes were blocked and the device was stored inside an aluminium box in order to avoid chemical degradation due to ambient lights. The device containing the droplets was then moved to a hot plate set on a confocal microscope stage (fig. 1b). The temperature of the hot plate was set to 56 °C to maintain a measured temperature of 37 ^{0}C inside the chamber. Using PTFE tubes, inlet 1 and outlet 3 were connected to the aqueous continuous phase syringe (the same one used for droplet generation) and the digestive fluid syringe, respectively. Outlet 4 was connected to the waste tank. Before thermal equilibrium was reached, the continuous phase was injected into the chamber at a flow rate of 50 µL min^{-1} to prevent air bubble development due to temperature rising. Then, the flow of the continuous phase was stopped and the reaction in the droplets was initiated by injecting digestive fluid via outlet 3 at a flow rate of 50 µL min^{-1}. This flow rate was kept constant throughout the reaction so that the digestive fluid in the chamber was theoretically renewed every 6 s. In practice, we measured that a steady-state concentration was typically reached after 1 min when replacing one solution by another one (results not shown).

Digestion was carried out with an intestinal phase or a gastric phase. For the intestinal phase, 10 mL of buffer solution (100 mM NaH_2PO_4 adjusted to pH 7.0) was mixed with pancreatic lipase at 4 mg mL^{-1} and a bile salt (sodium glycodeoxycholate) at 5 mg mL^{-1} to prepare a fresh intestinal digestive fluid forming an aqueous micellar solution due to the bile salt. This fluid was centrifuged at 1000g for 15 min to remove large residues before injection into the chamber.

The gastric phase experiments were run for 2 hours with a gastric digestive fluid containing 0.03 mg mL^{-1} lipase from *Aspergillus niger* (lipase AN), and 0.6 mg mL^{-1} pepsin in a 100 mM KCl buffer adjusted to pH 3.0. In order to get insights into the mechanisms of BC degradation during the gastric phase, three compositions of the gastric fluid were tested: i) lipase AN and pepsin, ii) lipase AN without pepsin, iii) only buffer with no enzymes.

2.5. Lipid monitoring

Tricaprylin (TC) droplets containing beta-carotene (BC) were observed during the digestion using a confocal microscope (Nikon A1+) with a 10× objective. The pinhole was set so that the thickness of the optical section was larger than the droplet initial diameter. Seven trapped droplets were monitored simultaneously in the field of view. A laser with an excitation wavelength of 488 nm and an emission window of 500-530 nm was used to obtain the

autofluorescence image of BC contained in the oil droplets. A transmitted light image for the droplet size was obtained simultaneously using the same excitation beam (Paddock, 2000).

For quantitative analysis, a calibration curve was constructed with five points. TC droplets with various BC concentrations (0 wt% as the negative control, 0.05, 0.2, 0.4, 0.5 wt%) were trapped in five different microfluidic devices to measure the fluorescence intensity due to BC autofluorescence (no dye is used in the experiments). The degradation of BC was also checked as a function of time for TC droplets containing BC. In those tests, the conditions were the same than for intestinal digestion, except only the buffer solution (pH 7.0) was injected instead of the digestive fluid. The measured fluorescence intensity was found to be proportional to the BC concentration inside the oil droplets, independently on the droplet size, and the degradation was found to be negligible (supplementary material S1).

Images were recorded automatically with an interval of 2 min or 5 min for intestinal or gastric digestion, respectively. Then, image analysis was performed to measure the size of the seven droplets in the field of view and their average fluorescence intensity. The droplet size was converted to the droplet volume, and the average fluorescence intensity was converted to BC concentration inside the oil droplet.

Note that the analysis was developed using pure chemicals (pure tricaprylin and a single bile salt) to avoid autofluorescence of undesirable molecules. As lipophilic micronutrients have specific fluorescent properties, it was found that real edible oils could be used with no fluorescence overlapping. In contrast, bile extract was difficult to use because it contains many unidentified molecules, resulting in fluorescence over a wide wavelength range (see the second article of this series).

For each system, two to three independent digestions were conducted with the monitoring of seven individual droplets for each digestion. A distinct microfluidic device was used for each digestion to ensure identical initial conditions. The variability of the measurements was very low between the seven droplets monitored during one digestion, so the error bar (plotted as the standard deviation) represents the variability of the two to three independent digestions.

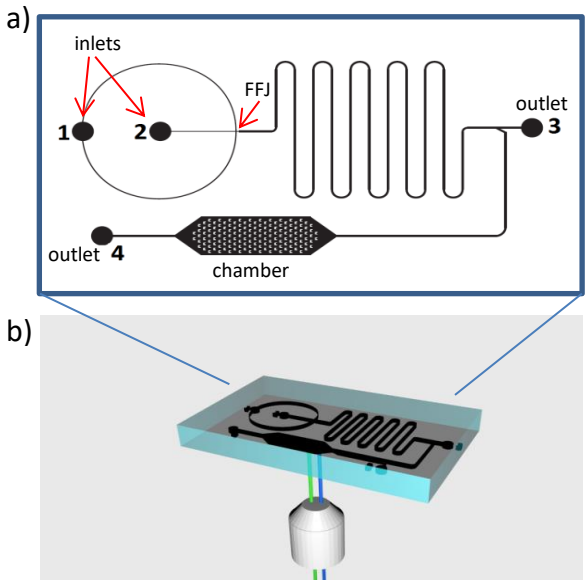

Fig. 1 a) Design of the PDMS microfluidic device for the generation, immobilization, and digestion of oil droplets. b) Real-time reactivity monitoring using confocal fluorescence microscopy.

3. Results and discussion

3.1. PDMS device fabrication

The PDMS device was constructed using two PDMS layers with different crosslinker concentrations (gradient technique). This technique resulted in a better association between the two PDMS parts compared to the plasma treatment method, eliminating the leakage during device operation while simplifying device fabrication. Moreover, this enabled the fabrication of 100% PDMS devices, which are lighter and easier to shape compared to devices made of PMMA, or using glass as the bottom part (Desai & Zaman, 2015; Huebner et al., 2009). In addition, PDMS has a broader transmission range (transmittance > 85%) than that of glass and PMMA, what is an advantage for the fluorescence analysis (Žukauskas et al., 2014).

3.2. PDMS surface modification

For the generation of oil droplets, the PDMS surface was rendered hydrophilic using the method proposed by Schneider et al. (Schneider et al., 2010). In this method, the benzophenone molecules diffuse into the PDMS matrix and play the role of the photoinitiator of UV polymerization, turning acrylic acid (pre-absorbed in the PDMS) into grafted hydrophilic poly(acrylic acid). The advantages of this method are to keep the geometry of the channel

unchanged and to provide a long persistency of the surface channel hydrophilicity. The post-treated devices still have an operational hydrophilic surface after one month of storage in pH 11 water at 4 °C. On the contrary, the layer coating technique changed the PDMS device geometry (Abate, Lee, Do, Holtze, & Weitz, 2008), and the hydrophilicity obtained via the plasma treatment method was only stable within 24 hours (Marze et al., 2014). The hydrophilic persistency we obtained enabled a systematic preparation of microfluidic devices that could be stored for later experiments.

3.3. Oil droplet immobilization

Oil droplets were generated in the flow focusing junction (FFJ) and trapped in the chamber of the microfluidic device (see fig. 1a). At the FFJ, the aqueous continuous phase entered perpendicularly to the oil disperse phase, facilitating the formation of oil droplets (supplementary video 1). Due to fluid handling limitation and instabilities, oil droplet size could not be modulated in our previous work (Marze et al., 2014). Here, the flow of initial polydisperse large oil droplets was led to the waste tank. When the desired droplet size was reached, the flow was switched to the chamber. Supplementary video 2 shows that this flow switch does not change the droplet size and the monodispersity. Thus, our new design with the chamber part and the FFJ part on the same chip leads to stable flows and enables droplet sorting so that only size-controlled ones enter the chamber. Moreover, its operation is more reliable, as the connection between the FFJ device and the chamber was a source of air/liquid leakage, flow disturbance, and droplet coalescence in the previous design (Marze et al., 2014). Nevertheless, one aspect needs to be discussed for this droplet generation approach. During the flow switch, the difference of hydrodynamic resistances between the two paths could disturb flow equilibrium. We optimized the geometry of the chip so that no droplet flow interruption was observed. Then, the continuous phase flow rate is only 50-fold higher than the oil flow rate, what is low compared to typical values required for viscous oils (200-fold higher). Indeed, the disturbance of the flow equilibrium comes from the disturbance of the pressure $\Delta P = R_h.Q$, (ΔP: applied pressure, R_h: hydrodynamic resistance, Q: flow rate). Thus, in the case of a low flow rate Q, the change in R_h will only have a small effect on the pressure ΔP. On the contrary, in the case of a high flow rate, the flow equilibrium would be more susceptible to the change in the hydrodynamic resistance. So the geometry (width, height and length of the channel) of the two branches has to be calculated carefully to suppress any hydrodynamic resistance difference.

Supplementary video 3 shows the trapping process of the oil droplets in the chamber. Most of the traps are filled with oil droplets. The number of traps was made large enough (150 traps) so that several droplet-free traps do not compromise the experiment. The average diameter of the oil droplets was manipulated to be 100 ± 5 µm in the different experiments.

The monodispersity of the droplet size in the same experiment is about 0.8%, crucial for repeatable measurements in the case of surface-dependent reactions. The total volume of the oil droplets represents approximately 0.7% of the total volume of the chamber. The oil droplets kept their spherical shape with no sign of surface deformations that could be caused by local defects of the hydrophilic treatment at the internal surface of the traps (Marze et al., 2014). The absence of hydrophilicity defects minimizes the contact between the oil droplets and the trap, maximizing the accessible droplet surface area. This validates this passive immobilization method by obstacles, which gives a high accessible droplet surface area and a high trapping efficiency compared to active trapping methods (optical tweezers, dielectrophoresis, acoustic trapping), which give a full accessible surface area but a low trapping efficiency (Hunt, Issadore, & Westervelt, 2007; Lee et al., 2009; Park & Chiou, 2011).

During device operation, the order of opening and blocking of outlets 3 and 4 must be respected to achieve monodisperse oil droplets trapping in the chamber. In this condition, neither air bubbles nor droplet coalescence are observed inside the device during oil droplet generation and trapping. This open-close procedure for the outlets is a very efficient method to control the flow of oil droplets while simplifying the device structure, avoiding the use of pneumatic valves (Unger, Chou, Thorsen, Scherer, & Quake, 2000), or torque-actuated valves as proposed by Weibel et al. (Weibel et al., 2005). Also, our method does not require infusion-withdraw pumps to control the droplet flow (Huebner et al., 2009).

Our device was also used to obtain multiple droplets trapped in a single trap for coalescence studies. Monodisperse TC droplets of 90 µm diameter were generated and trapped. In this case, the droplet size was smaller than that of the trapping space, resulting in two droplets per trap. This configuration was used to study the effect of droplet coalescence during the gastric phase on the subsequent intestinal droplet digestion (supplementary material S2).

Similar PDMS devices were proposed to immobilize aqueous droplets for enzymatic reactions (Huebner et al., 2009), or oil droplets for lipid digestion (Marze et al., 2014). In this work, oil droplets containing BC were used to study the release (or degradation) kinetics of BC during the intestinal phase (or the gastric phase), as reported in the following section.

3.4. Kinetics of beta-carotene release during intestinal digestion

In order to illustrate the application of the device for release kinetics of lipophilic molecules, immobilized TC droplets with added 0.2 wt% BC were generated (single droplet trapping) and then submitted to intestinal digestion conditions. The kinetics of lipid digestion and beta-carotene release were monitored simultaneously in real time with a confocal fluorescence microscope setup.

Figs. 2 and supplementary video 4 show the evolution of oil droplet size and BC concentration as a function of digestion time. The droplet volume and BC concentration are reported as normalized values (relative to the initial values) in order to simplify the comparisons. Droplet volume is reduced over time (fig. 2a) because triglyceride lipolysis produces fatty acids and monoglycerides that exit the droplet as they are soluble in the aqueous micellar phase. The kinetics is similar to the one reported by Marze et al. (Marze et al., 2014). A discussion of the effect of lipase concentration on digestion kinetics is found in the supplementary material S3.

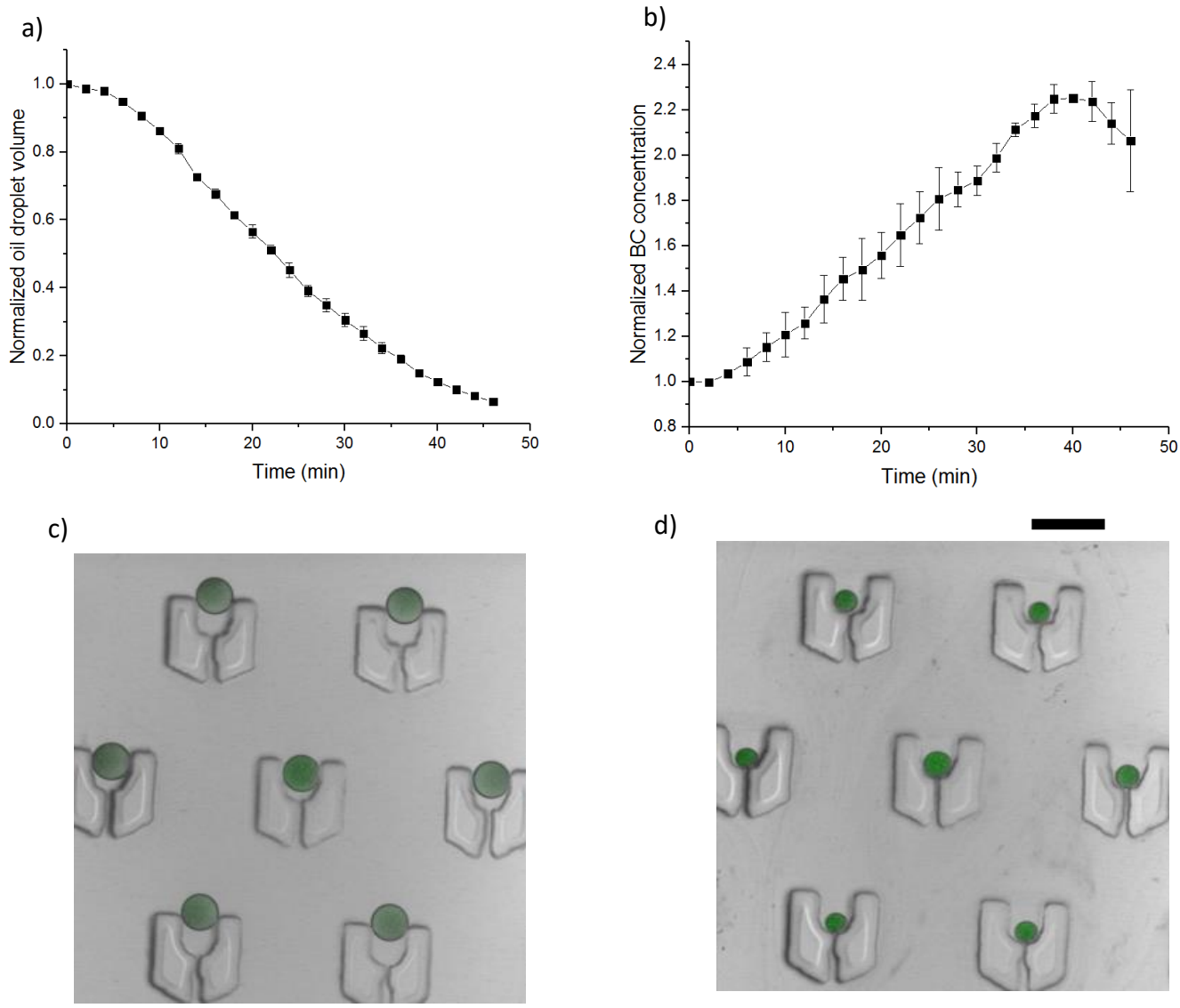

Fig. 2 a) Evolution of the normalized volume of TC droplets during intestinal digestion. b) Evolution of the normalized beta-carotene concentration inside TC droplet during intestinal digestion. c) d) Images of TC droplets containing beta-carotene at digestion times: 0, 24 min, respectively. The scale bar represents 200 µm.

As evidenced in fig. 2b, a trend for BC concentration in oil droplets is observed. Indeed, BC concentration mainly increases during digestion, although it reaches a maximum and then decreases near the end of the digestion. This means that the reduction rate of oil droplet volume is faster than the solubilizing rate of BC out of the droplets. Thus, BC concentrates inside the reducing droplets. At the end of the digestion, triglyceride digestion rate slows down but not the BC release rate (fig. 3), resulting in the decreasing trend for BC concentration.

From the data presented in figs. 2a and 2b, BC quantity released out of the droplets (incorporated in the micellar phase) can be calculated for quantitative analysis, using the mass balance:

$$m_{RL} = m_{Di} - m_D \quad \text{with} \quad m_D = V_D C \qquad (1)$$

Here m_{RL} is the mass of BC released from the oil droplet, m_{Di} is the initial mass of BC inside the oil droplet, m_D is the mass of BC inside the oil droplet, V_D is the volume of the oil droplet and C is the concentration of BC inside the oil droplet, determined from the fluorescence intensity using the calibration curve. All values are presented in normalized form.

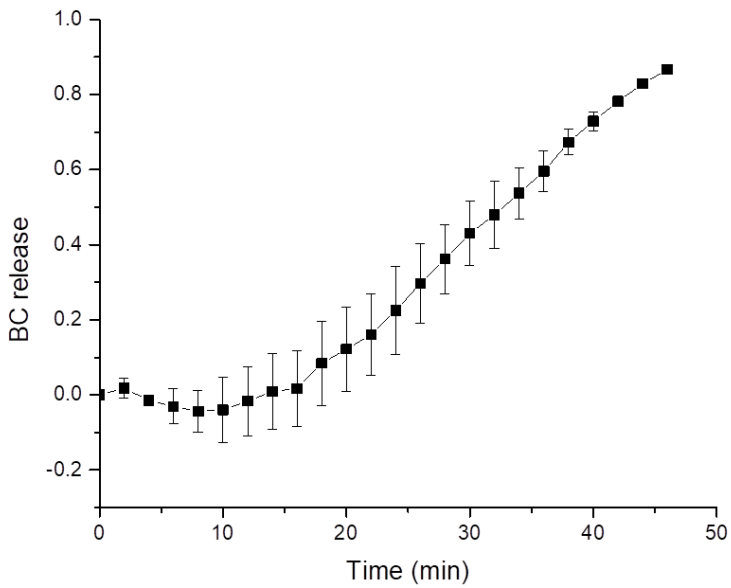

Fig. 3 Evolution of the BC proportion released from TC droplets during intestinal digestion (bioaccessibility).

Kinetics of BC release during intestinal digestion is shown in fig. 3. Note that negative values can be obtained at the beginning of the digestion where both kinetics are slow. Due to these initial low releases, the determination of BC concentration is indeed sensitive to the precision of the calibration curve, and to fluctuations of the laser intensity. Nevertheless, the error bars in fig. 3 show that these values are not significantly different from zero.

In the current non-static digestion conditions with continuous renewal of the intestinal digestive fluid, bile salt micelles come in large excess compared to the digestion products and BC to solubilize. That explains the higher release of BC (almost 90% bioaccessibility) than those typically reported for static digestion of emulsions in the literature (Nik, Corredig, & Wright, 2011; Mutsokoti et al., 2017; Salvia-Trujillo et al., 2017).

Fig. 4 shows the relation between the micellar solubilization of BC and of the lipolytic products during intestinal digestion, providing a better view of their kinetic interplay. The black dash line represents the “balance” case of identical BC and lipid release rate. In order to analyze the curves in fig. 4 in terms of relative kinetics, three tangent lines are added, representing different BC release regimes. The first order derivative of the curve $\frac{dRL_{BC}}{dRL_{LP}}$ (slope of the tangent line) is equal to the release rate ratio between BC and lipids:

$$\frac{dRL_{BC}}{dRL_{LP}} = \frac{\frac{dRL_{BC}}{dt}}{\frac{dRL_{LP}}{dt}} = \frac{\text{BC release rate}}{\text{Lipid release rate}} \qquad (2)$$

In which, $\frac{dRL_{BC}}{dt}$ and $\frac{dRL_{LP}}{dt}$ are the first order derivative of BC and lipid release as a function of digestion time, respectively.

The slopes on the non-linear curve reveal three different kinetic regimes. In the first part (beginning of the digestion), the slope of the tangent line is smaller than 1 ($\frac{dRL_{BC}}{dRL_{LP}}$<1), showing that BC release rate is slower than that of lipids. This caused the increase of BC concentration inside the oil droplets. In the middle part, a balanced regime can be observed. In the third part (end of the digestion), the release rate of BC becomes faster than that of the lipids ($\frac{dRL_{BC}}{dRL_{LP}}$ >1), explaining the decrease trend of BC concentration observed near the end of the digestion (fig. 2b).

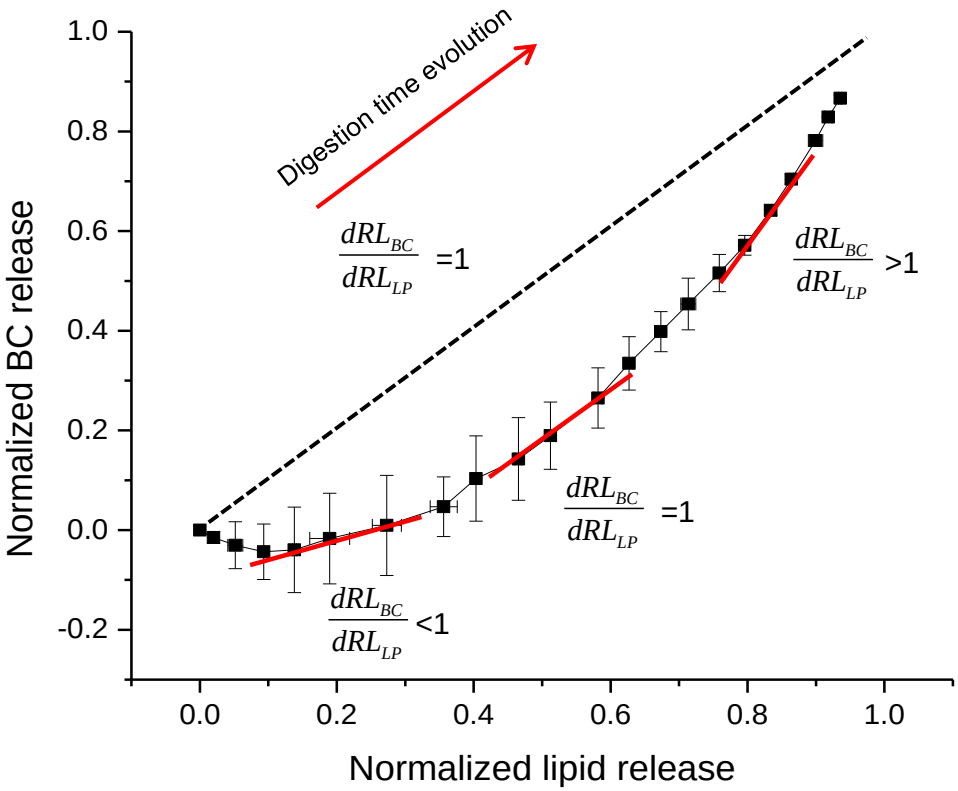

Fig. 4 Relation between the normalized mass release of BC and of lipids.

3.5. Beta-carotene degradation in gastric conditions

For this study, the same protocols (as in section 3.4.) were used except the intestinal fluid was replaced by a gastric fluid. Fig. 5a shows the evolution of the droplet volume in gastric conditions using various gastric fluid compositions. The decrease of the TC droplet volume was only seen with the gastric fluid containing both lipase AN and pepsin. This decrease reached up to 50% of the initial droplet volume, what is higher than the usual lipolysis degree (10-30%) measured during the gastric phase *in vivo* (Favé, Coste, & Armand, 2004). This difference could be explained by the absence of droplet coalescence, that has an essential effect in the stomach *in vivo* (Li et al., 2012). Marze et al. reported 10-20% TC droplet volume reduction (initial size of 137 µm) obtained after 55 min of gastric digestion using a similar device (Marze et al., 2014). The larger initial droplet size, shorter duration of the gastric phase, and the absence of pepsin in the gastric fluid could explain the lower lipolysis degree of tricaprylin. Fig. 5a also shows the role of pepsin, as no reduction of the droplet volume was obtained in the absence of pepsin in the gastric fluid. Indeed, pepsin hydrolyses the β-lactoglobulin protein initially coating the droplet surface, facilitating the adsorption and activity of lipase AN for triglyceride lipolysis.

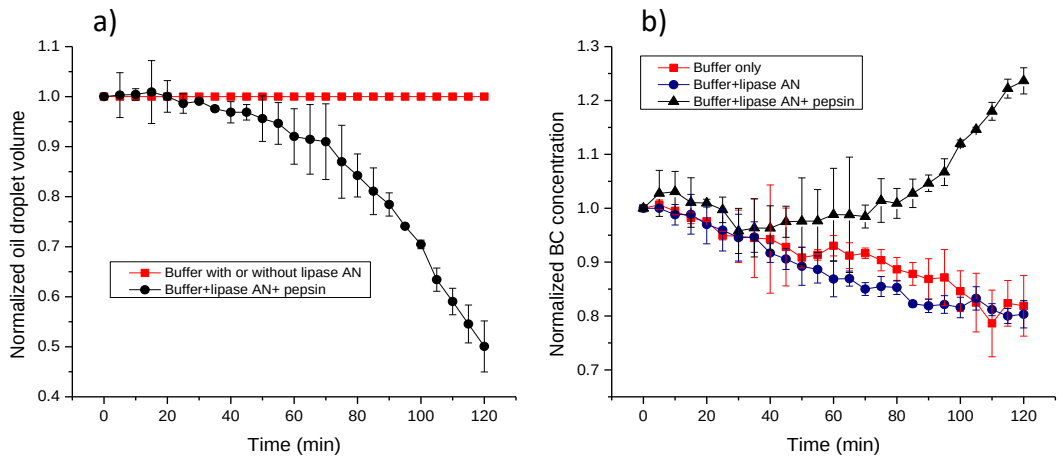

Fig. 5 a) Evolution of the normalized volume of TC droplets, and b) evolution of the normalized BC concentration inside TC droplets during gastric digestion with different gastric fluid compositions. In the cases of buffer with or without lipase AN, no change in droplet volume was observed.

Fig. 5b shows the evolution of BC concentration inside the TC droplets during the gastric phase. In the absence of pepsin (lipase AN or buffer only), as there was no change in droplet volume, the 20% decrease of BC concentration reveals a 20% degradation of BC. This result shows that this degradation is mostly due to the low pH condition (pH 3.0) during the gastric phase, as the addition of lipase AN has no significant effect on BC degradation. A 25% degradation of BC in emulsions during the gastric phase was reported by Kopec et al. (Kopec, Gleize, Borel, Desmarchelier, & Caris-Veyrat, 2017), regardless of the presence or absence of pepsin. In the case with lipase AN and pepsin, two different regions are observed, with a BC concentration decreasing trend during the first 40 min, followed by an increasing trend until the end of the gastric phase. During the first 40 min, there is almost no reduction of the droplet volume, thus the decrease of the BC concentration reveals the degradation of BC inside the oil droplet. The kinetics of BC degradation is similar than in the absence of pepsin, confirming the limited effect of pepsin on BC degradation. The region of increasing BC concentration is observed during the reduction of the droplet volume. In this region, it is likely that both BC degradation and BC release contribute to the kinetics.

In order to discriminate each contribution, we assumed that the degradation of BC in the presence of pepsin is similar to the case without pepsin (buffer+lipase AN). Thus, both BC degradation and BC total loss (degradation+release) could be calculated from the data presented in figs. 5a and 5b. Then, the BC release could be deduced. The evolutions of the normalized total loss and release of BC during the gastric phase are shown in fig. 6. This

result shows that BC release during the gastric phase is low (about 20%), occurring significantly only after 100 min. This was not expected as BC is highly hydrophobic and should only release in the presence of bile salt micelles. However, a similar result (up to 30% BC release) was reported in the case of highly stable MCT emulsions using decaglycerol monolaurate as the emulsifier (Liu, Hou, Lei, Chang, Gao, 2012). The absence of coalescence might explain the efficiency of the release, although another factor is needed, such as the possibility of tricaprylin lipolytic products (or decaglycerol monolaurate in Liu, Hou, Lei, Chang, Gao, 2012) to form micelles able to solubilize BC.

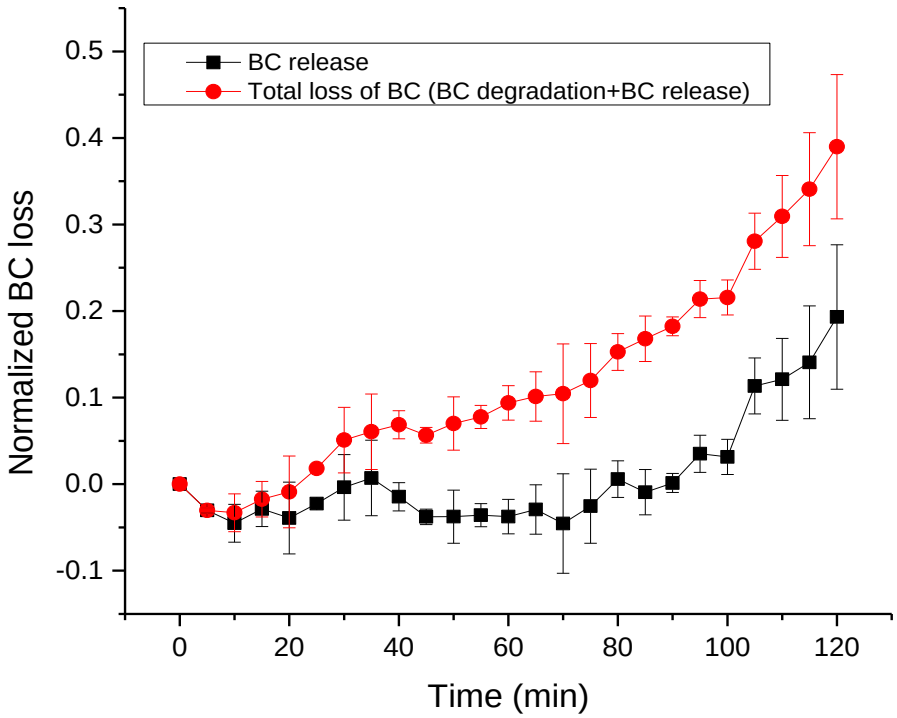

Fig. 6 Normalized BC total loss (BC degradation+BC release) and BC release during gastric digestion, in the case of buffer+ lipase AN+pepsin.

4. Conclusion

This work shows that the real-time kinetics of lipophilic bioactive molecules can be studied using droplet microfluidics, as monitored by confocal fluorescence microscopy. The design and fabrication of the setup were optimized to obtain a long hydrophilicity persistency of the channel surface, and to facilitate the oil droplet generation and trapping. The development of an open-close procedure of the outlets enabled the generation and trapping of oil droplets on

a single chip, and solved the issue of flow instabilities by compensating for the high oil viscosity. These results show the potential of immobilized oil droplets to screen the reactivity of lipophilic molecules. In the second article of this series and in subsequent works, the use of this lab on a chip platform will be extended to different edible oils and fat-soluble micronutrients. A comprehensive study of the degradation of antioxidant lipophilic molecules during the gastric phase will be carried out as well. The whole approach can be generalized to screen the reactivity of lipophilic molecules in the context of bioavailability studies which are conducted in nutrition, pharmacology, and toxicology.

References

Abate, A. R., Lee, D., Do, T., Holtze, C., & Weitz, D. A. (2008). Glass coating for PDMS microfluidic channels by sol-gel methods. *Lab on a Chip*, *8*(4), 516–518.

Desai, D., & Zaman, M. H. (2015). Continuous flow microfluidic solution for quantitative analysis of active pharmaceutical ingredient content and kinetic release. *Analytical Methods*, *7*(5), 1914–1923.

Favé, G., Coste, T. C., & Armand, M. (2004). Physicochemical properties of lipids: new strategies to manage fatty acid bioavailability. *Cellular and Molecular Biology (Noisy-Le-Grand, France)*, *50*(7), 815–831.

He, T., Liang, Q., Zhang, K., Mu, X., Luo, T., Wang, Y., & Luo, G. (2011). A modified microfluidic chip for fabrication of paclitaxel-loaded poly(l-lactic acid) microspheres. *Microfluidics and Nanofluidics*, *10*(6), 1289–1298.

Heus, F., Giera, M., De Kloe, G. E., Van Iperen, D., Buijs, J., Nahar, T. T., … Kool, J. (2010). Development of a microfluidic confocal fluorescence detection system for the hyphenation of nano-LC to on-line biochemical assays. *Analytical and Bioanalytical Chemistry*, *398*(7–8), 3023–3032.

Huebner, A., Bratton, D., Whyte, G., Yang, M., Demello, A. J., Abell, C., & Hollfelder, F. (2009). Static microdroplet arrays: A microfluidic device for droplet trapping, incubation and release for enzymatic and cell-based assays. *Lab on a Chip*, *9*(5), 692–698.

Huebner, A. M., Abell, C., Huck, W. T. S., Baroud, C. N., & Hollfelder, F. (2011). Monitoring a Reaction at Submillisecond Resolution in Picoliter Volumes. *Analytical Chemistry, 83*, 1462–1468.

Hunt, T. P., Issadore, D., & Westervelt, R. M. (2007). Integrated circuit/microfluidic chip to programmably trap and move cells and droplets with dielectrophoresis. *Lab on a Chip*, *8*(1), 81–87.

Kopec, R. E., Gleize, B., Borel, P., Desmarchelier, C., & Caris-Veyrat, C. (2017). Are lutein, lycopene, and β-carotene lost through the digestive process? *Food and Function*, *8*(4), 1494–1503.

Lee, J., Teh, S. Y., Lee, A., Kim, H. H., Lee, C., & Shung, K. K. (2009). Single beam acoustic trapping. *Applied Physics Letters*, *95*(7), 2–4.

Li, Y., Kim, J., Park, Y., & McClements, D. J. (2012). Modulation of lipid digestibility using structured emulsion-based delivery systems: Comparison of in vivo and in vitro measurements. *Food and Function*, *3*(5), 528–536.

Liu,Y., Hou, Z., Lei, F., Chang, Y., & Gao, Y. (2012). Investigation into the bioaccessibility and microstructure changes of β-carotene emulsions during in vitro digestion. *Innovative Food Science and Emerging Technologies, 15*, 86–95.

Marquis, M., Renard, D., & Cathala, B. (2012). Microfluidic generation and selective degradation of biopolymer-based Janus microbeads. *Biomacromolecules*, *13*(4), 1197–1203.

Marze, S., Algaba, H., & Marquis, M. (2014). A microfluidic device to study the digestion of trapped lipid droplets. *Food Funct.*, *5*(7), 1481–1488.

Marze, S. (2015). Bioaccessibility of lipophilic micro-constituents from a lipid emulsion. *Food and Function*, *6*(10), 3218–3227.

Mata, A., Fleischman, A. J., & Roy, S. (2005). Characterization of polydimethylsiloxane (PDMS) properties for biomedical micro/nanosystems. *Biomedical Microdevices*, *7*(4), 281–293.

Mongersun, A., Smeenk, I., Pratx, G., Asuri, P., & Abbyad, P. (2016). Droplet Microfluidic Platform for the Determination of Single-Cell Lactate Release. *Analytical Chemistry*, *88*(6), 3257–3263.

Mutsokoti, L., Panozzo, A., Pallares Pallares, A., Jaiswal, S., Van Loey, A., Grauwet, T., & Hendrickx, M. (2017). Carotenoid bioaccessibility and the relation to lipid digestion: A kinetic study. *Food Chemistry*, *232*, 124–134.

Nik, A. M., Corredig, M., & Wright, A. J. (2011). Release of lipophilic molecules during in vitro

digestion of soy protein-stabilized emulsions. *Molecular Nutrition and Food Research*, *55*(SUPPL. 2), 278–289.

Paddock, S. W. (2000). Principles and Practices of Laser Scanning Confocal Microscopy. *Molecular Biotechnology*, *16*(2), 127–150.

Park, S. Y., & Chiou, P. Y. (2011). Light-driven droplet manipulation technologies for lab-on-a-chip applications. *Advances in OptoElectronics*, *2011*(1).

Šalić, A., Tušek, A., & Zelić, B. (2012). Application of microreactors in medicine and biomedicine. *Journal of Applied Biomedicine*, *10*(3), 137–153.

Salvia-Trujillo, L., Verkempinck, S. H. E., Sun, L., Van Loey, A. M., Grauwet, T., & Hendrickx, M. E. (2017). Lipid digestion, micelle formation and carotenoid bioaccessibility kinetics: Influence of emulsion droplet size. *Food Chemistry*, *229*, 653–662.

Scheuble, N., Iles, A., Wootton, R. C. R., Windhab, E. J., Fischer, P., & Elvira, K. S. (2017). Microfluidic Technique for the Simultaneous Quantification of Emulsion Instabilities and Lipid Digestion Kinetics. *Analytical Chemistry*, *89*(17), 9116–9123.

Schneider, M. H., Willaime, H., Tran, Y., Rezgui, F., & Tabeling, P. (2010). Wettability patterning by UV-initiated graft polymerization of poly(acrylic acid) in closed microfluidic systems of complex geometry. *Analytical Chemistry*, *82*(21), 8848–8855.

Tan, J., Xu, J. H., Li, S. W., & Luo, G. S. (2008). Drop dispenser in a cross-junction microfluidic device: Scaling and mechanism of break-up. *Chemical Engineering Journal*, *136*(2–3), 306–311.

Unger, M. A., Chou, H. P., Thorsen, T., Scherer, A., & Quake, S. R. (2000). Monolithic microfabricated valves and pumps by multilayer soft lithography. *Science*, *288*(5463), 113–116.

Wang, K., Lu, Y. C., Xu, J. H., & Luo, G. S. (2009). Determination of dynamic interfacial tension and its effect on droplet formation in the T-shaped microdispersion process. *Langmuir*, *25*(4), 2153–2158.

Weibel, D. B., Kruithof, M., Potenta, S., Sia, S. K., Lee, A., & Whitesides, G. M. (2005). Torque-actuated valves for microfluidics. *Analytical Chemistry*, *77*(15), 4726–4733.

Whitesides, G. M., Ostuni, E., Takayama, S., Jiang, X., & Ingber, D. E. (2001). Soft Lithography in Biology and Biochemistry. *Annual Review of Biomedical Engineering*, *3*(1), 335–373.

Windbergs, M., & Weitz, D. A. (2011). Drug Dissolution Chip (DDC): A microfluidic approach for drug release. *Small*, *7*(21), 3011–3015.

Žukauskas, A., Batavičiūtė, G., Ščiuka, M., Jukna, T., Melninkaitis, A., & Malinauskas, M. (2014). Characterization of photopolymers used in laser 3D micro/nanolithography by means of laser-induced damage threshold (LIDT). *Optical Materials Express*, *4*(8), 1601.

Calibration curve for beta-carotene concentration and degradation due to the intestinal buffer at pH 7.0

A factor that may have an effect on the real-time measurement of fluorescence is BC degradation due to the repeated laser excitation at 488 nm. This figure shows the effect of a pulse excitation (500 ms pulse duration) repeated every 2 min on the fluorescence intensity of TC droplets with added 0.2 wt% BC. The measured fluorescence intensity decreased by 1% and 5% after 25 and 60 excitations (corresponding to 50 and 120 min), respectively. About 25 time points were used to cover the digestion kinetics, so by the end of the experiment, only 1% of the variation of the fluorescence intensity could be attributed to degradation, which was neglected.

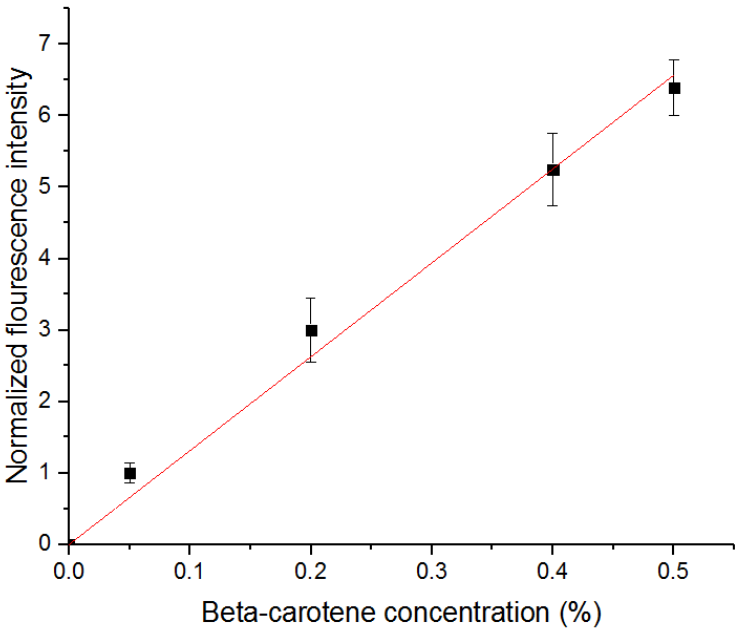

Calibration curve of the average fluorescence intensity in the TC droplets as a function of BC concentration (R^2=0.9902).

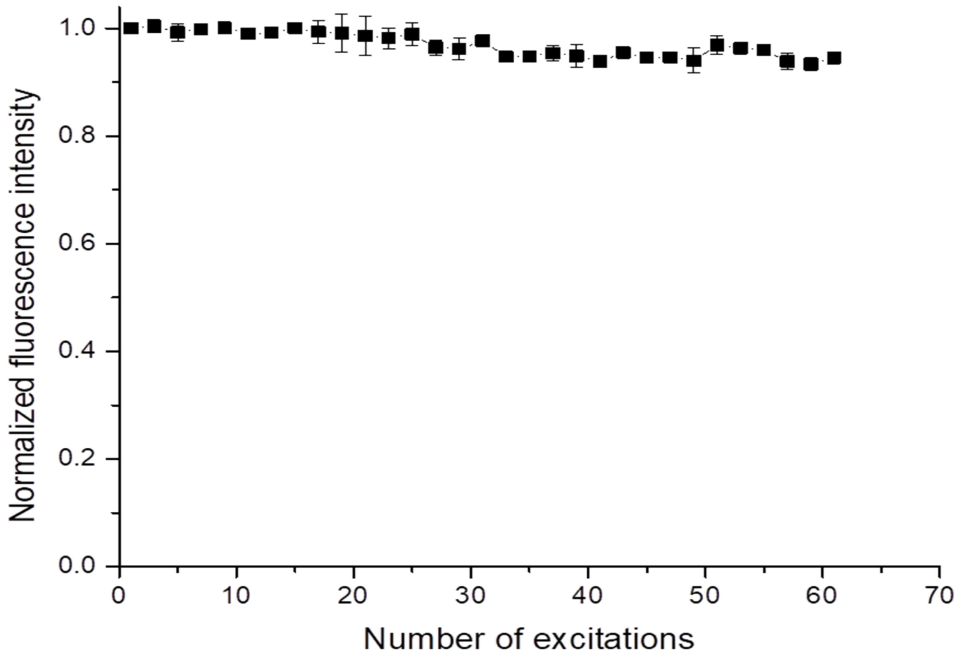

Evolution of the average fluorescence intensity in the TC droplets exposed to the intestinal buffer at pH 7.0 as a function of the number of laser excitations.

Gastric coalescence effect on intestinal digestion

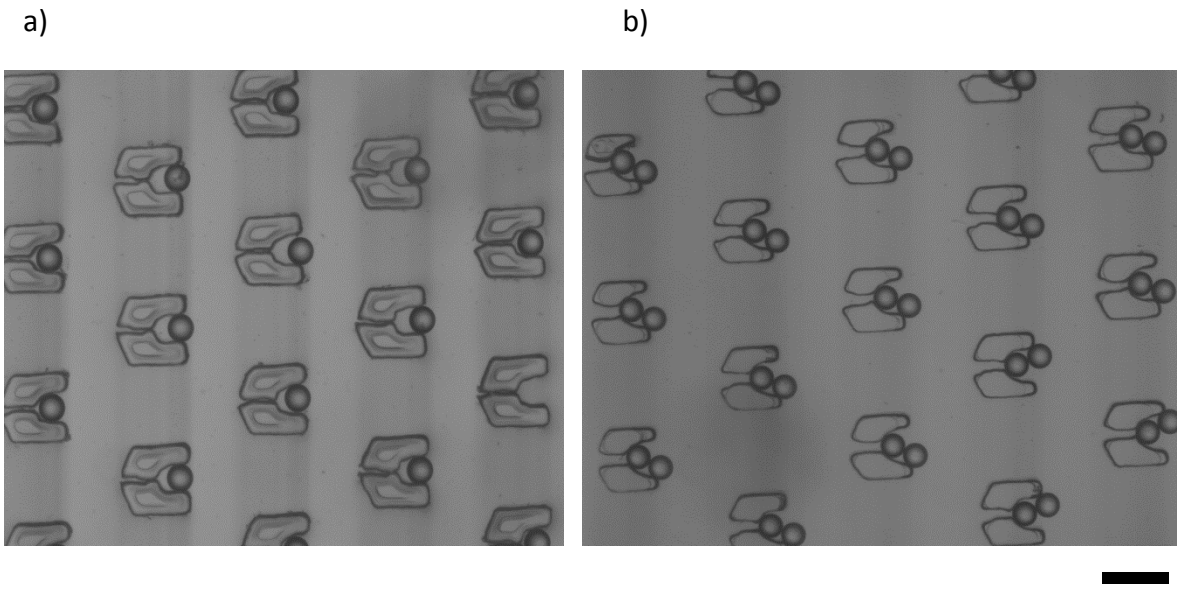

Fig. 1 Oil droplets trapped inside the chamber: a) Single droplet trapping, b) double droplet trapping. The scale bar represents 200 µm.

For this experiment, two droplets of 90 µm per trap were subjected to gastrointestinal digestion to test the effect of coalescence. A gastric phase (buffer+lipase AN+pepsin) of 60 min preceded the intestinal phase. Fig. 2a) shows the droplets at different times of gastrointestinal digestion. Coalescence occurred in some but not all traps near the end of the gastric phase. Thus intestinal digestion could be monitored simultaneously for both uncoalesced (diameter 90 µm) and coalesced (diameter 112 µm) droplets. Fig. 2b) shows the different kinetics of intestinal digestion in these two cases. The rate of volume decrease for the uncoalesced droplets is higher than that for the coalesced droplet (rate ratio of about 1.28). This is likely a surface area effect, as gastric coalescence caused the fusion of two droplets into a single larger droplet, reducing the surface area compared to separate droplets. The surface area is indeed reduced by a factor $2*(90/112)^2$, that is about 1.29, explaining the ratio between the rates of volume decrease.

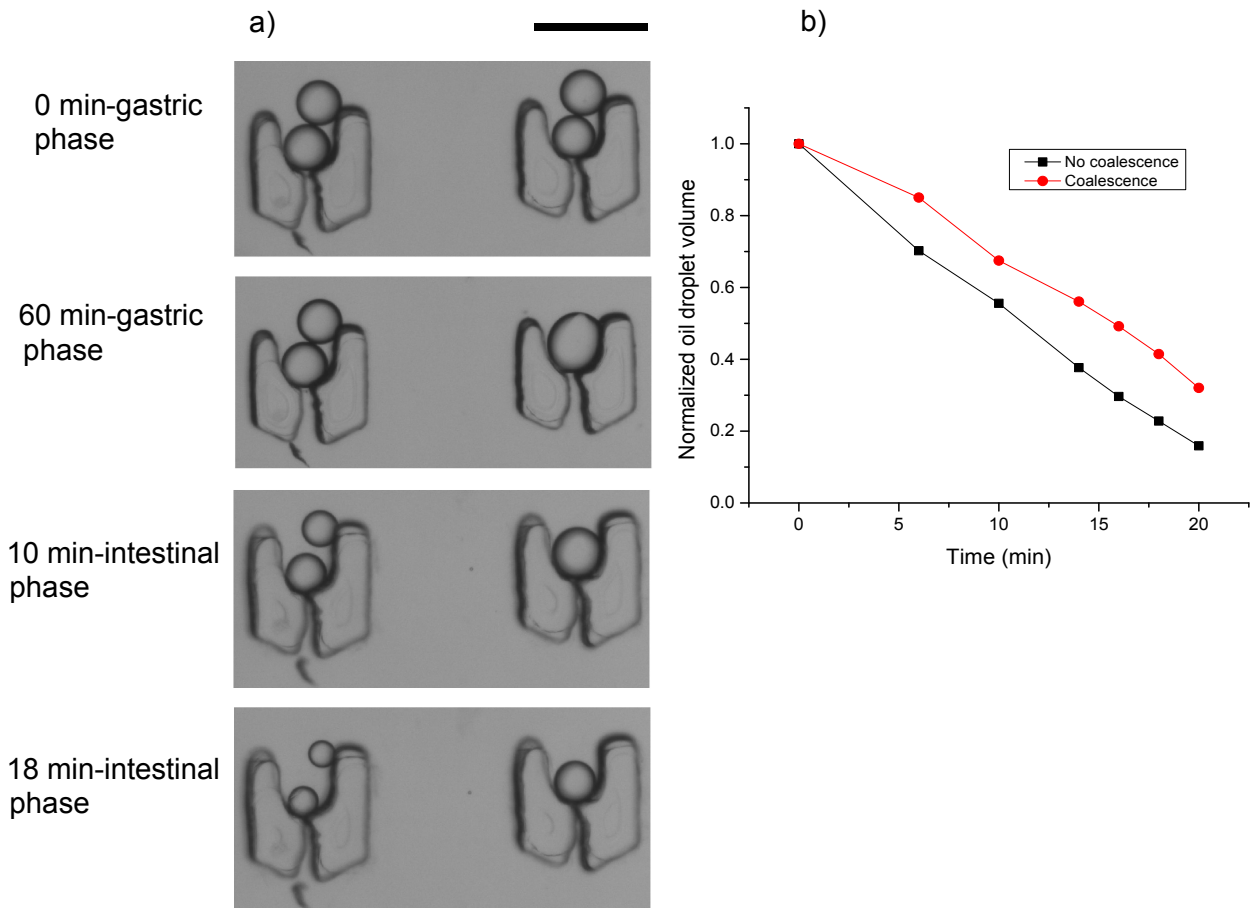

Fig. 2 a) Images of uncoalesced and coalesced droplets during gastrointestinal digestion, b) Evolution of the normalized volume of TC droplets during intestinal digestion (with or without coalescence during the gastric phase). The black scale bar is 200 µm.

Effect of lipase concentration on the intestinal digestion of oil droplets

Oil droplets were subjected to intestinal digestion with lower lipase concentrations (0.1 mg mL^{-1}) to compare with the normal case of lipase concentration 4 mg mL^{-1}. Tricaprylin digestion with the two lipase concentrations is shown below. In the case of the low lipase concentration (0.1 mg mL^{-1}), a longer lag phase is observed at the beginning of the digestion. This lag phase likely represents the time needed to saturate the oil droplet surface with lipase. Thus, a lower lipase concentration results in a longer lag phase. When the curve for the lower lipase concentration (0.1 mg mL^{-1}) is shifted by 10 min (lag phase), both curves superimpose (see figure). This result means that as long as lipase saturates the droplet surface, lipid digestion proceeds with the same kinetics regardless of the lipase concentration in the digestive fluid.

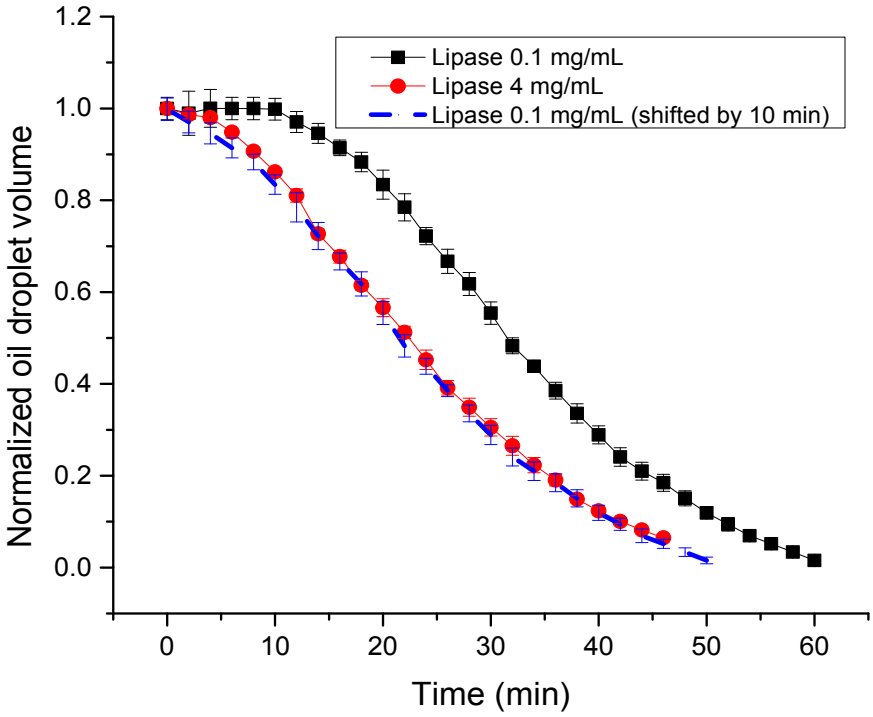

Effect of lipase concentration on intestinal digestion of TC oil droplets